Computational ECG reconstruction and validation from high-resolution optical mapping

Conner Herndon[1], Ilija Uzelac[1], James T Farmer[1], Flavio Fenton[1]

[1] Georgia Institute of Technology, Atlanta, Georgia, USA

Abstract

Here we present a series of improvements to the optical mapping electrocardiogram (OM-ECG), a reconstruction of the ECG based on transmembrane voltages measured on the surface of the heart. We compare our predicted OM-ECG with a pseudo-ECG concurrently measured with platinum leads surrounding the heart in-vitro. We find that the surface optical mapping of transmembrane voltages is sufficient for capturing important morphology in the ECG and moreover intramural propagation waves due to the specific transmembrane voltage sensitive dye used. Methods concerning OM-ECG reconstruction are detailed and discussed in comparison to the pseudo-ECG.

1. Introduction

The heart provides a constantly changing charge density which results in the electrocardiogram (ECG), a periodic change in the electric potential outside the body. Allowing quick diagnoses of arrhythmia, the ECG has proven itself an invaluable heuristic tool for medical practitioners for over a century. Despite its success, the drawback of the ECG is in its inability to make specific claims about the heart's electrophysiology. [1] Much work has been devoted to the "forward problem of electrocardiography", whereby one calculates the electric potential developed by simulated cardiac systems to better understand the origin of the ECG. [2]

Optical mapping is an experimental technique that allows measurement of transmembrane voltages over the entire surface of the heart. With knowledge of these transmembrane voltages, one may more easily bridge the gap between cellular phenomena and global behavior. In this study, we apply models used in numerical simulations of cardiac tissue to optical mapping data to test the both the validity of the models and the strength of their predictions.

2. Methods

Experiments conformed to the current Guide for Care and Use of Laboratory Animals published by the National Institute of Health (NIH Publication No. 85-23, revised 1996) and approved by the Office of Research and Integrity Assurance at Georgia Tech. New Zealand white rabbits (4) were anesthetized with ketamine/xylazine/acempromazine (17/9/0.9 mg/kg, respectively) and then injected with heparin (300 U/kg). After five minutes, euthanasia was induced with pentobarbital (120 mg/kg). Hearts were quickly excised via left thoracotomy and perfused retrogradely through the aorta with cardioplegic solution gassed with 95% O_2 and 5% CO_2. Afterwards the heart was immersed in a chamber kept at 37.0$\pm$0.3°C and perfused with Tyrode's solution gassed with 95% O_2 and 5% CO_2, kept at 37.0$\pm$0.3°C. Pressure was monitored of about 60 mmHg and controlled with a peristaltic pump. The hearts were then stained for 15-20 minutes with a 100 mL Tyrode solution containing 40μmol/L of voltage-sensitive dye Di-4-ANBDQPQ [JPW6003], previously dissolved in ethanol (24.4 mg/mL). Heart motion was suppressed perfusing the heart with Tyrodes solution containing 2-5 μmol/L of blebbistatin for 20-30 minutes prior data acquisition. Hearts were fixed in a glass imagining chamber containing Tyrodes solution and illuminated by three red LEDs of 660 nm center wavelength (LED Engin), each coupled with band emission filter 650/10 nm (Edmund Optics). Epicardial voltage signals (emitted fluorescence signals) were filtered through 700 nm long pass emission filter and recorded using a back-illuminated EMCCD camera (Photometrics Evolve 128) at 500 fps at resolution of 128$\times$128 pixels that corresponds to spatial resolution of the heart surface of about 250 μm/pixel. Optical mapping signals were analyzed using a stacking procedure (ensemble averaging) [3] of up to 400 beats to increase signal to noise ratio in order to avoid filtering that would degrade information of interest particularly at higher frequencies.

2.1. Pseudo-ECG

Two pairs of planar platinum electrodes (12$\times$60 mm), right-left (R-L) and base-apex (B-A), shown in Figure 1, were connected to Arduino ECG shield board (Olimex) stacked on the Arduino Due development board. The electrodes were placed around the heart in a plane perpen-

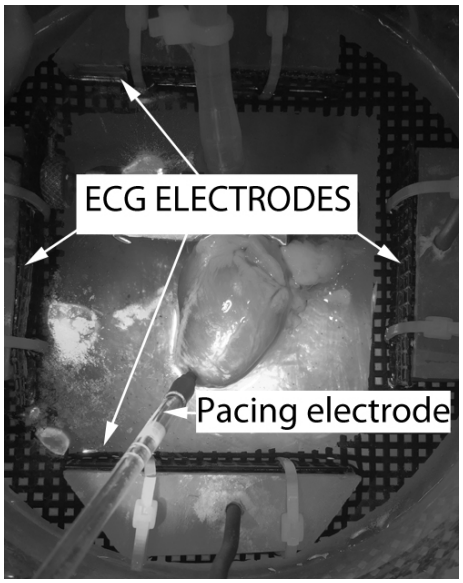

Figure 1. Image showing rabbit's heart, perfused in a heated oval chamber with four platinum electrodes placed around and pacing electrode at the apex.

dicular to camera's vantage. The two channel ECG signals were digitized with Arduino Due internal 12bit A/D converter at 2000 sps. On the PC side custom written software in MATLAB was used to communicate with the Arduino board, and to visualize and record the pseudo ECG-signals. Optical mapping images were simultaneously recorded with pseudo-ECG signals.

2.2. ECG Reconstruction from Optical Mapping

According to the bidomain formulation, the cardiac volume Ω_H contains two overlapping domains corresponding to the intra- and extracellular regions of the cell with an associated electric potential $u_i(\boldsymbol{r})$ and $u_e(\boldsymbol{r})$, respectively. A transmembrane voltage V_m may be then defined for every position $\boldsymbol{r}$ in the cardiac volume

$$V_m = u_i - u_e. \tag{1}$$

This transmembrane voltage acts as an equivalent cardiac source allowing us to solve the Poisson equation for the electric potential

$$\boldsymbol{\nabla}^2\varphi \propto \begin{cases} 0, & \boldsymbol{r} \notin \Omega_H \\ -\boldsymbol{\nabla}^2 V_m, & \boldsymbol{r} \in \Omega_H. \end{cases} \tag{2}$$

As detailed in [4–6], this potential may also be expressed as an integral when evaluated outside of the heart

$$\varphi(\boldsymbol{r}) \propto \int\limits_{\Omega_H} d^3r' \, \frac{\boldsymbol{\nabla}'^2 V_m(\boldsymbol{r}')}{|\boldsymbol{r}-\boldsymbol{r}'|}. \tag{3}$$

This integral requires full knowledge of transmembrane voltages V_m throughout the heart; however, optical mapping measures only V_m along the surface of the heart. With intelligent lead placement, we may approximate this volume integral as an integral over the visible area of the heart with a correction term. We may write Equation 3 as

$$\varphi(\boldsymbol{r}) \propto \int d^3r' \, \frac{\boldsymbol{\nabla}'^2 V_m(\boldsymbol{r}')}{\sqrt{\Delta s^2 + \Delta z^2}}, \tag{4}$$

where $\Delta s^2 = (x-x')^2 + (y-y')^2$ and $\Delta z = (z-z')$. Consider the case $\Delta z \ll \Delta s$. Then to first order in $\Delta z/\Delta s$,

$$\begin{aligned} \varphi(\boldsymbol{r}) &\propto \int d^3r' \, \frac{\boldsymbol{\nabla}'^2 V_m(\boldsymbol{r}')}{\Delta s\sqrt{1+(\Delta z/\Delta s)^2}} \\ &\propto \int d^3r' \, \frac{\boldsymbol{\nabla}'^2 V_m(\boldsymbol{r}')}{\Delta s}\left[1 - \frac{1}{2}\left(\frac{\Delta z}{\Delta s}\right)\right]. \end{aligned} \tag{5}$$

If we assume V_m to be nearly constant through z, then we may name the first term $\varphi_{(2D)}$, the 2D contribution to the potential

$$\varphi(\boldsymbol{r}) \propto \varphi^{(2D)}(\boldsymbol{r}) - \frac{1}{2}\int d^3r' \, \frac{\boldsymbol{\nabla}'^2 V_m}{\Delta s}\left(\frac{\Delta z}{\Delta s}\right). \tag{6}$$

The difference between potentials evaluated at two points φ_1 and φ_2 with the same z-coordinate is then

$$\begin{aligned} \Delta\varphi &= \varphi_1 - \varphi_2 \\ &\propto \Delta\varphi^{(2D)} - \frac{1}{2}\int d^3r' \, \boldsymbol{\nabla}'^2 V_m\left[\frac{\Delta z}{\Delta s_1^2} - \frac{\Delta z}{\Delta s_2^2}\right]. \end{aligned} \tag{7}$$

We then see that the potential calculated from optical mapping is a reasonable approximation when $\Delta z \ll \Delta s_{1,2}$. With origin at the center of the heart, this requirement is satisfied when $z = 0$ and the $x-$, $y-$coordinate of the probe far from the heart.

3. Results

In the post-processing workflow before the OM-ECG calculation, a region of interest (ROI) containing the heart and placement of OM-ECG electrodes are selected as presented in Figure 2.

3.1. Region of Interest for OM-ECG Leads

Although the integral in Equation 3 allows quick determination of the electric potential at a point, the pseudo-ECG leads concurrently measured during the experiment occupied non-negligible area. It is assumed that Tyrode's solution is a homogeneous and relatively good conductor, and

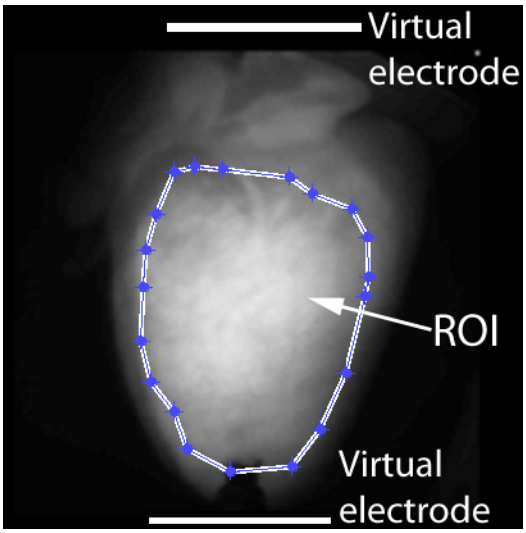

Figure 2. For OM-ECG calculation ROI is selected from the surface of the ventricle while virtual electrodes are simulated to correspond to the same position and as real pseudo-ECG electrodes.

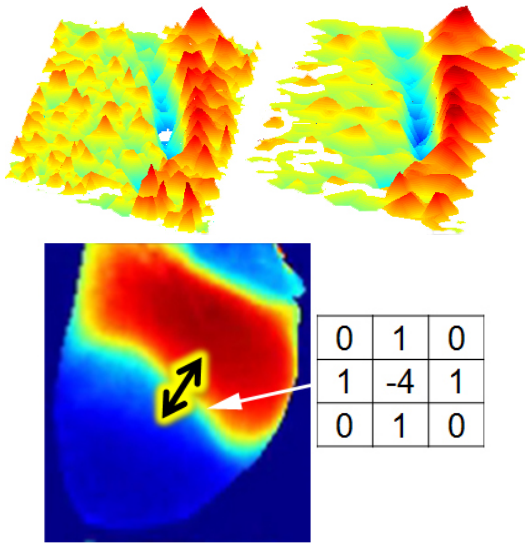

Figure 3. Surface plots comparing 128×128 (top left) and 64×64 (top right) pixel images for a single frame of optical mapping data. Optical mapping data (bottom) were convolved with the Laplacian in Equation 8.

that the pseudo-ECG leads are very good conductors. To simulate the real pseudo-ECG leads in the OM-ECG calculation, the unipolar electric potential is calculated at every point (pixel) within each OM-ECG lead. These potentials are averaged for each lead, and the OM-ECG is expressed as the difference between these averaged potentials, analogous to the bipolar ECG measurement. Averaging the electric potential for each lead not only more accurately reflects the pseudo-ECG configuration, but also reduces noise.

3.2. Optical Mapping Resolution

We performed optical mapping of transmembrane voltages at 500 fps over a 128×128 pixel grid for our experiments. Since the integral in Equation 3 is a function of the Laplacian applied to images of the surface transmembrane voltage, OM-ECG is strongly dependent on the spatial rate of transmembrane voltage dispersion. Therefore, for a surface propagating activation wavefront it is beneficial that there are sharp transitions between polarized and depolarized regions, ideally on the pixel-to-pixel scale, as shown in Figure 3. As the emission spectra of JPW-6003 voltage dye in near-infra red region (above 700 nm), emitted fluorescence not only emanates from the epicardial surface but also from deeper ventricular wall layers reaching the depth of 4 mm [7], since tissue is mostly transparent in infrared spectrum. Since emitted fluorescence is generally very weak, a fast optics system must be used in connection with the camera that results in a shallow, sub-millimeter depth of field. As a consequence emitted florescence light cannot be focused from each transmural layer which results in a blurred image, effectively lowering resolution from 128×128. We convolved the 3×3 Laplacian convolution operator

$$\begin{pmatrix} 0 & 1 & 0 \\ 1 & -4 & 1 \\ 0 & 1 & 0 \end{pmatrix} \tag{8}$$

with each image in OM-ECG calculation. The Laplacian operator is effectively an edge detection filter when applied to an image, and to emphasize waterfront detection in the optical mapping data, images are sub-sampled to the lower resolution 64×64 pixels. Figure 3 shows the significant improvement when the Laplacian operator is applied to wavefront detection of sub-sampled images of 64×64 pixels versus the original image of 128×128 pixels.

3.3. Normalization for DC Offset

Unipolar OM-ECG potential amplitudes are strongly biased by the distance from unipolar OM-ECG leads to the ROI of the heart, resulting in a different DC offset and unipolar OM-ECG amplitudes that affect final OM-ECG calculation. To counteract the effect of relative distances between heart and the electrodes, DC offset is subtracted and unipolar potentials are normalized before their subtraction. This procedure is consistent with real ECG medical devices where only DC part of the ECG signal from each lead is filtered out as DC levels greatly vary and depend on many parameters, rendering the ECG apparatus incapable of measuring DC levels. Figure 4 shows images

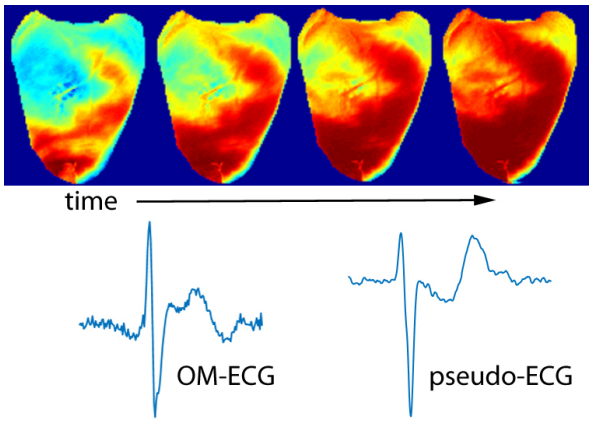

Figure 4. Top: four frames from optically mapped transmembrane voltages in a rabbit ventricle. Bottom: reconstructed OM-ECG (left) and *in-vitro* recorded pseudo-ECG. Despite the heterogeneous wave propagation, the OM-ECG reproduces characteristic ECG morphology.

of a propagating wavefront from a pacing electrode located at the apex along with pseudo-ECG and OM-ECG signals. In this specific example, the activating wavefront does not propagate strictly along the surface. Strong intramural propagation is visible resulting in a surface that does not depolarize from the planar surface wave, but from deeper intra-ventricular layers. Despite the intramural propagation, OM-ECG calculation shows almost perfectly reconstructed matching pseudo-ECG signal. We contribute this agreement to the nature of the voltage dye used in that its near-infra red emission spectra makes it possible to record optical signal not only from the surface but across the ventricular wall.

4. Limitations

Although one may theoretically predict the electric potential due to a localized charged density, not all transmembrane voltages may be measured simultaneously. Optical mapping yields surface imaging of epicardial transmembrane voltages which is blind of intramural dynamics. As expressed in Equation 7, the volume integral may be written as the integral over the surface with a correction that requires the OM-ECG leads be placed far from the heart. When intramural and mid-myocardial dynamics are not similar to those on the epicardial surface, the OM-ECG is unable to predict extra-cardiac electric potential.

Future work will involve whole-heart numerical simulations combining surface transmembrane voltage data with forecasting methods. These simulations will give an estimate for intramural dynamics, allowing for more accurate OM-ECG calculation. Discrepancies between the OM-ECG and *in-vitro* measured pseudo-ECG will illuminate further these dynamics, allowing for improved simulations.

5. Acknowledgements

This work was performed with support from NSF grant number 1341190 and GT-PURA (Georgia Tech Presidential Undergraduate Research Award) number 4106F07.

References

[1] Dupre A, Viedau S, Iazzo P. Handbook of Cardiac Anatomy, Physiology, and Devices. Second edition. Springer Science + Business Media, 2009.

[2] MacFarlane P, van Oosterom A, Pahlm O, Kligfield P, Janse M, Camm J (eds.). Comprehensive Electrocardiology. Springer, 2011.

[3] Uzelac I, Fenton F. Robust framework for quantitative analysis of optical mapping signal without filtering. Computing in Cardiology, 2015; .

[4] Geselowitz D. On the theory of the electrocardiogram. Proceedings of the IEEE 1989;77(6).

[5] Franzone P, Pavarino L, Scacci S. Mathematical Cardiac Electrophysiology, volume 13. Springer, 2014.

[6] Uzelac I, Herndon C, Farmer J, Fenton F. Electrocardiogram reconstruction from high resolution voltage optical mapping. IEEE Engineering in Medicine and Biology, 2016; .

[7] Walton RD, Mitrea BG, Pertsov AM, Bernus O. A novel near-infrared voltage-sensitive dye reveals the action potential wavefront orientation at increased depths of cardiac tissue. Proceedings of the 31st Annual International Conference of the IEEE Engineering in Medicine and Biology Society: Engineering the Future of Biomedicine, EMBC, 2009; 4523–4526.